Numerical investigation of wave fields and currents in a coastal engineering case study

GIOVANNI CANNATA, LUCA BARSI, CHIARA PETRELLI, FRANCESCO GALLERANO
Department of Civil, Constructional and Environmental Engineering
"Sapienza" University of Rome
Via Eudossiana 18, 00184
ITALY
giovanni.cannata@uniroma1.it https://www.dicea.uniroma1.it/en/users/giovannicannata

Abstract: - In this paper, we present a Boussinesq type model which is able to simulate wave fields and nearshore currents in coastal regions characterized by morphologically complex coastal lines and irregular seabed and by the presence of coastal structures. The proposed model solves the integral contravariant form of the fully non-linear Boussinesq equations, from deep water up to just seaward of the surf zones, and the non-linear shallow water equations, in the surf zone, on curvilinear boundary conforming grids. By the proposed model, a detailed representation is carried out of the hydrodynamic phenomena which contribute to generate the silting process at the entrance of the Cetraro harbour (Italy). Furthermore, the effects produced by the placement of a groin updrift of the head of the main jetty on coastal hydrodynamics and sediment transport are evaluated.

Key-Words: - coastal engineering, Boussinesq equations, contravariant formulation, shock-capturing method, breaking waves, nearshore currents

1 Introduction

In the design and management of coastal structures, an evaluation is needed regarding the effects that such structures have on the sediment transport, seabed erosion and coastline changes. These phenomena are related to the combined action of wave motion and wave-induced nearshore currents. Consequently, in the design and management of coastal structures it is a priority to adequately represent the wave motion and nearshore currents.

In order to produce an effective representation of the wave motion and nearshore currents, two-dimensional wave resolving models can be seen as an interesting compromise between classical methodologies (which are based on the use of radiation stresses) and recent methodologies based on three-dimensional approaches [3][9-11]. The two-dimensional wave resolving models are based on the combined solution of the Boussinesq equations for the representation of wave propagation from deep water up to just seaward of the surf zone and the non-linear shallow water equations for the representation of wave propagation in the surf [15][19]. These models are able to take into account the non-linear wave-wave interactions, the fully coupled wave-current interactions and the breaking related near shore currents.

The modelling of hydrodynamics over computational domains representing the complexity of real case morphologies can be done by using computational grids obtained by the intersection of boundary conforming coordinate lines. Using curvilinear computational grids, the equations can be written in contravariant formulation [12][16]. Curvilinear models based on the solution of the contravariant non-linear shallow water equations have been presented by [2][4][18], whereas curvilinear models based on the solution of the contravariant Boussinesq equations have been presented by [7-8][17].

In this paper, we present a Boussinesq type model whose equations are written in a contravariant formulation and solved on curvilinear grids representing the complex morphology of the real case studies. The equations at the base of this model are derived starting from the fully non-linear formulation of the Boussinesq equations proposed by [5], which retain the term related to the second order vertical vorticity. The proposed model solves the fully nonlinear Boussinesq equations from deep water up to just seaward of the surf zones and the non-linear shallow water equations in the surf zones. The model is able to represent wave evolution in coastal regions, wave breaking, breaking induced longshore and rip currents and effects produced by offshore structures on the hydrodynamics. An upwind WENO (Weighted Essentially Non-Oscillatory) scheme [6] for the solution of the motion equations on generalized curvilinear grids is used in this work. The conservative terms are solved by a high-order finite

volume shock-capturing scheme in which an exact Riemann solver is involved [21].

The proposed model is used to numerically investigate the wave motion dynamics and the wave-induced nearshore currents in the coastal region opposite Cetraro harbour (Italy). By the proposed model, a detailed representation is carried out of the hydrodynamic phenomena which contribute to generate the silting process at the entrance of the Cetraro harbour (Italy). Furthermore, the effects produced by the placement of a groin updrift of the head of the main jetty on coastal hydrodynamics and sediment transport are evaluated.

2 Problem Formulation

Let $H = h + \eta$ be the total local water depth, where h is the local still water depth and η is the local surface displacement. Using a Taylor expansion of the velocity about an arbitrary distance from the still water surface, σ, and assuming zero horizontal vorticity [5][14][22], the vertical distribution of the horizontal velocity can be written as

$$\vec{u} = \vec{u}_{z=\sigma} + \vec{u}_2(z) \tag{1}$$

where $\vec{u}_{z=\sigma}$ is the horizontal velocity at an arbitrary distance from the still water level and $\vec{u}_2(z) = (\sigma - z)\nabla[\nabla \cdot (h\vec{u}_{z=\sigma})] + [(\sigma^2/2) - (z^2/2)]\nabla(\nabla \cdot \vec{u}_{z=\sigma})$ consists of the second order terms in depth power expansion of the velocity vector in which ∇ is the two-dimensional differential operator defined as $\nabla = (\partial/\partial x, \partial/\partial y)$ in a Cartesian reference system.

We define the vectors $\vec{v} = H\vec{u}_{z=\sigma}$ and $\vec{w} = H\vec{u}_2$, in which $\vec{u}_2$ is the depth averaged value of $\vec{u}_2(z)$. The explicit expression of $\vec{w}$ is

$$\vec{w} = H\left\{\left[\frac{\sigma^2}{2} - \frac{1}{6}(h^2 - h\eta + \eta^2)\right]\nabla\left(\nabla \cdot \frac{\vec{v}}{H}\right) + \left[\sigma + \frac{1}{2}(h - \eta)\right]\nabla\left[\nabla \cdot \left(h\frac{\vec{v}}{H}\right)\right]\right\} \tag{2}$$

By introducing the auxiliary variable $\vec{v}^*$ as

$$\vec{v}^* = \vec{v} + H\vec{V}' \tag{3}$$

The fully non-linear Boussinesq equations expressed in a conservative form in a two-dimensional Cartesian system, where the dependent variables are H and $\vec{v}^*$, are

$$\frac{\partial H}{\partial t} + \nabla \cdot (\vec{v}) = -\nabla \cdot (\vec{w}) \tag{4}$$

$$\frac{\partial \vec{v}^*}{\partial t} + \nabla \cdot \left(\frac{\vec{v} \otimes \vec{v}}{H}\right) + G\nabla\frac{H^2}{2} = GH\nabla h - \vec{R} - \frac{\vec{r}}{H}\nabla \cdot \vec{s} + \frac{\partial H}{\partial t}\vec{V}' - H\vec{V}'' - H\vec{T} - H\vec{W} \tag{5}$$

where $\otimes$ is the tensor product between vectors, G is the constant of gravity, $\vec{V}'$, $\vec{V}''$ and $\vec{T}$ are the dispersive terms obtained by retaining terms up to $O(\mu^2)$ and $O(\varepsilon\mu^2)$ in depth power expansions of the horizontal velocity according to [22], $\vec{W}$ is the term related to the approximation to the second order of the vertical component of the vorticity according to [5] and $\vec{R}$ is the bottom resistance term. The above-mentioned terms are given by

$$\vec{V}' = \frac{1}{2}\sigma^2\,\nabla\left(\nabla \cdot \frac{\vec{v}}{H}\right) + \sigma\nabla\left(\nabla \cdot h\frac{\vec{v}}{H}\right) - \nabla\left[\frac{1}{2}\eta^2\left(\nabla \cdot \frac{\vec{v}}{H}\right) + \eta\left(\nabla \cdot h\frac{\vec{v}}{H}\right)\right] \tag{6}$$

$$\vec{V}'' = \nabla\left[\frac{\partial}{\partial t}\left(\frac{\eta^2}{2}\right)\nabla \cdot \frac{\vec{v}}{H}\right] + \nabla\left[\frac{\partial \eta}{\partial t}\nabla \cdot \left(h\frac{\vec{v}}{H}\right)\right] \tag{7}$$

$$\vec{T} = \nabla\left\{(\sigma - \eta)\left(\frac{\vec{v}}{H} \cdot \nabla\right)\left[\nabla \cdot \left(h\frac{\vec{v}}{H}\right)\right] + \frac{1}{2}(\sigma^2 - \eta^2)\left(\frac{\vec{v}}{H} \cdot \nabla\right)\left(\nabla \cdot \frac{\vec{v}}{H}\right)\right\} + \frac{1}{2}\nabla\left\{\left[\nabla \cdot \left(h\frac{\vec{v}}{H}\right) + \eta\nabla \cdot \frac{\vec{v}}{H}\right]^2\right\} \tag{8}$$

$$\vec{W} = \hat{\imath}\left[\Omega\left(-\frac{s_y}{H}\right) - \Theta\left(-\frac{r_y}{H}\right)\right] + \hat{\jmath}\left[\Omega\left(\frac{s_x}{H}\right) - \Theta\left(\frac{r_x}{H}\right)\right] \tag{9}$$

in which $\Omega = \left[\frac{\partial}{\partial x}\left(\frac{r_y}{H}\right) - \frac{\partial}{\partial y}\left(\frac{r_x}{H}\right)\right]$ and $\Theta = \left[\frac{\partial}{\partial x}\left(\frac{s_x}{H}\right) - \frac{\partial}{\partial y}\left(\frac{s_y}{H}\right)\right]$.

Let us rewrite equations (4) and (5) in contravariant formulation in a two-dimensional system of generalized curvilinear coordinates.

We consider the coordinate transformation $x^l = x^l(\xi^1, \xi^2)$ from the Cartesian coordinate system $\vec{x}$ to the curvilinear coordinate system $\vec{\xi}$ (note that superscripts indicate the generic component and not powers). Let $\vec{g}_{(l)} = \partial\vec{x}/\partial\xi^l$ be the covariant base vectors and $\vec{g}^{(l)} = \partial\xi^l/\partial\vec{x}$ the contravariant base vectors. The covariant and contravariant metric coefficients are given respectively by $g_{lm} = \vec{g}_{(l)} \cdot \vec{g}_{(m)}$ and $g^{lm} = \vec{g}^{(l)} \cdot \vec{g}^{(m)}$. The Jacobian of the transformation is given by $\sqrt{g} = \sqrt{|g_{lm}|}$ where $|\ |$ denotes the determinant of the covariant metric coefficients g_{lm}. The transformation relationships between vector $\vec{v}$ in the Cartesian coordinate system and its contravariant, v^l, and covariant, v_l, components in the curvilinear coordinate system are given by

$$v^l = \vec{g}^{(l)} \cdot \vec{v} \quad ; \quad \vec{v} = v^l \vec{g}_{(l)}$$

$$v_l = \vec{g}_{(l)} \cdot \vec{v} \quad ; \quad \vec{v} = v_l \vec{g}^{(l)} \tag{10}$$

In the following equations, a comma with an index in a subscript stand for covariant differentiation. The covariant derivative is defined as $v^l_{,m} = \frac{\partial v^l}{\partial \xi^m} + \Gamma^l_{mk} v^k$, where Γ^l_{mk} is the Christoffel symbol [1] given by

$$\Gamma^l_{mk} = \vec{g}^{(l)} \frac{\partial \vec{g}_{(k)}}{\partial \xi^m} \tag{11}$$

Let v^{*l} be the l-th contravariant component of the vector $\vec{v}^*$ defined by equation (3). v^{*l} reads

$$v^{*l} = v^l + HV'^l \tag{12}$$

Let ΔA be the area of the generic surface element and $\vec{\tilde{g}}^{(l)} = \vec{g}^{(l)}(\xi_0^1, \xi_0^2)$ the contravariant base vector defined at point $P_0(\xi_0^1, \xi_0^2) \in \Delta A$. Let also $\lambda_k(\xi^1, \xi^2) = \vec{\tilde{g}}^{(l)} \cdot \vec{g}_{(k)}$ be the covariant component of $\vec{\tilde{g}}^{(l)}$ where $\vec{g}_{(k)} = \vec{g}_{(k)}(\xi^1, \xi^2)$. The integral contravariant form of the continuity equation (4) and momentum equation (5) can be expressed as

$$\iint_{\Delta A} \frac{\partial H}{\partial t} dA + \int_L v^m n_m dL = \iint_{\Delta A} \left(w^l\right)_{,l} dA \tag{13}$$

$$\begin{aligned}
&\iint_{\Delta A} \vec{\tilde{g}}^{(l)} \cdot \vec{g}_{(k)} \frac{\partial \vec{v}^*}{\partial t} dA + \\
&\int_L \left(\vec{\tilde{g}}^{(l)} \cdot \vec{g}_{(k)} \frac{v^k v^m}{H} + G \vec{\tilde{g}}^{(l)} \cdot \vec{g}_{(k)} \frac{H^2}{2} \right) n_m dL = \\
&\iint_{\Delta A} \vec{\tilde{g}}^{(l)} \cdot \vec{g}_{(k)} GH g^{km} h_{,m} dA - \iint_{\Delta A} \vec{\tilde{g}}^{(l)} \cdot \vec{g}_{(k)} R^k dA \\
&- \iint_{\Delta A} \vec{\tilde{g}}^{(l)} \cdot \vec{g}_{(k)} \frac{v^k}{H} (w^m)_{,m} dA \\
&+ \iint_{\Delta A} \vec{\tilde{g}}^{(l)} \cdot \vec{g}_{(k)} \frac{\partial H}{\partial t} V'^k dA \\
&- \iint_{\Delta A} \vec{\tilde{g}}^{(l)} \cdot \vec{g}_{(k)} H V''^k dA - \iint_{\Delta A} \vec{\tilde{g}}^{(l)} \cdot \vec{g}_{(k)} H T^k dA \\
&- \iint_{\Delta A} \vec{\tilde{g}}^{(l)} \cdot \vec{g}_{(k)} H W^k dA
\end{aligned} \tag{14}$$

where L is the contour line of ΔA and n_m is the outward unit vector normal to ΔA. In equation (13) the second term on the left-hand side is the flux term. In equation (14) the second term on the left-hand side is the flux term, the first term on the right-hand side is the source term related to the bottom slope, the second term on the right-hand side, R^l, is the bottom resistance term approximated by a quadratic law as in [20]. Expressions for terms w^l, V'^l, V''^l, T^l and W^l are given by

$$\begin{aligned}
s^l = &\\
&(h+\eta) \left\{ \left[\frac{\sigma^2}{2} - \frac{1}{6}(h^2 - h\eta + \eta^2) \right] g^{lm} \left[\left(\frac{v^k}{H} \right)_{,k} \right]_{,m} \right. \\
&\left. + \left[\sigma + \frac{1}{2}(h - \eta) \right] g^{lm} \left[\left(h \frac{v^k}{H} \right)_{,k} \right]_{,m} \right\}
\end{aligned} \tag{15}$$

$$\begin{aligned}
V^l = &\\
&\frac{\sigma^2}{2} g^{lm} \left[\left(\frac{\partial}{\partial t} \left(\frac{v^k}{H} \right) \right)_{,k} \right]_{,m} + \sigma g^{lm} \left[\left(h \frac{\partial}{\partial t} \left(\frac{v^k}{H} \right) \right)_{,k} \right]_{,m} \\
&- g^{lm} \left[\frac{1}{2} \eta^2 \left(\frac{\partial}{\partial t} \left(\frac{v^k}{H} \right) \right)_{,k} + \eta \left(h \frac{\partial}{\partial t} \left(\frac{v^k}{H} \right) \right)_{,k} \right]_{,m}
\end{aligned} \tag{16}$$

$$\begin{aligned}
V'^l = &\frac{1}{2} \sigma^2 \, g^{lm} \left[\left(\frac{v^k}{H} \right)_{,k} \right]_{,m} + \sigma g^{lm} \left[\left(h \frac{v^k}{H} \right)_{,k} \right]_{,m} - \\
&g^{lm} \left[\frac{1}{2} \eta^2 \left(\frac{v^k}{H} \right)_{,k} + \eta \left(h \frac{v^k}{H} \right)_{,k} \right]_m
\end{aligned} \tag{17}$$

$$V''^l = g^{lm} \left[\frac{\partial}{\partial t} \left(\frac{\eta^2}{2} \right) \left(\frac{v^k}{H} \right)_{,k} \right]_{,m} + g^{lm} \left[\frac{\partial \eta}{\partial t} \left(h \frac{v^k}{H} \right)_{,k} \right]_{,m} \tag{18}$$

$$\begin{aligned}
T^l = &\\
&g^{lm} \left\{ (\sigma - \eta) \left(\frac{v^i}{H} \left[\left(h \frac{v^k}{H} \right)_{,k} \right]_{,i} \right) + \right. \\
&\left. \frac{1}{2} (z_\alpha^2 - \eta^2) \left(\frac{v^i}{H} \left[\left(\frac{v^k}{H} \right)_{,k} \right]_{,i} \right) \right\}_{,m} + \\
&\frac{1}{2} g^{lm} \left\{ \left[\left(h \frac{v^k}{H} \right)_{,k} + \eta \left(\frac{v^k}{H} \right)_{,k} \right]^2 \right\}_{,m}
\end{aligned} \tag{19}$$

$$W^l = \left(\varepsilon^{mi} g_{ip} \frac{v^p_{,m}}{H} \right) \varepsilon^{jl} \frac{s_j}{H} + \left(\varepsilon^{mi} g_{ip} \frac{w^p_{,m}}{H} \right) \varepsilon^{jl} \frac{v_j}{H} \tag{20}$$

in which ε^{mi} is equal to $\frac{1}{\sqrt{g}}$, $-\frac{1}{\sqrt{g}}$ or 0 respectively if (m, i) is an even permutation, odd permutation or if the two indices are equal.

Equations (13) and (14) represent the integral expressions of the fully non-linear Boussinesq equations in contravariant formulation in which the Christoffel symbols are absent. These equations are accurate to $O(\mu^2)$ and $O(\varepsilon\mu^2)$ in dispersive terms and retain the conservation of potential vorticity up to $O(\mu^2)$, in accordance with the formulation proposed by [5].

Equations (13) and (14) are solved by a hybrid finite volume-finite difference scheme [7-8]. Convective terms and terms related to the free surface elevation gradient are discretized by a high order finite-volume upwind WENO scheme [6]; dispersive terms and the term related to the second order vertical

vorticity are discretized by a finite-difference scheme. The upwind WENO scheme needs a flux calculation at the cell interfaces. These fluxes are calculated by means of the solution of a Riemann problem. An exact Riemann solver is used in this work [21]. No additional dissipative term to improve the modelling of breaking related energy decay and breaking induced near shore recirculation is used in this paper.

3 Simulation of wave field and currents in the coastal region opposite the Cetraro harbour (Italy)

The Cetraro harbour, located in a natural inlet subtended by Punta La Testa, was built at the beginning of the Fifties of the last century. Only after the last works performed from 2000, the harbour has taken on its final configuration, with water depth up to 5m in the wide stretch of water close to the main jetty, equipped with a more than 20m wide dock. From a management point of view, the main issue of the Cetraro harbour is the significant silting which affects the harbour entrance.

As shown in Figure 1, from the meteo-marine study performed starting from the time series recorded by the Cetraro wavemeter, it turns out that the coastal storm mainly responsible for the solid transport phenomena (i.e. those associated to wave trains with significant height greater than 0.5m) primarily come from the West sector (occurrence frequency around equal to 30% of the events, corresponding to 110days/year), and secondarily from the other directional sector (less than 5% for each sector).

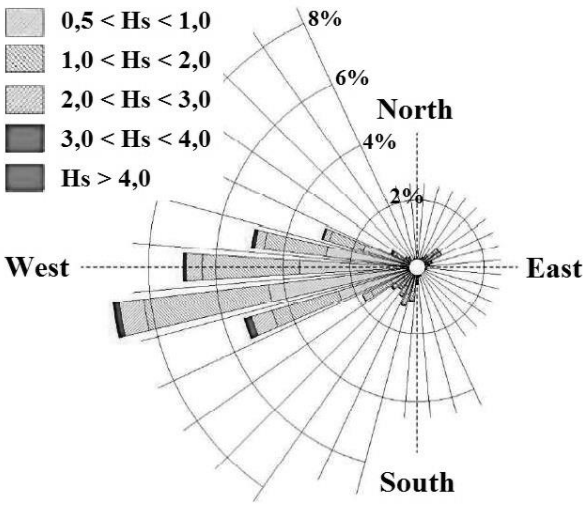

Fig. 1: Directional annual distribution of the wave events in the coastal region opposite the Cetraro harbour.

The proposed model is used to study the hydrodynamic fields in a coastal region opposite a portion of coastline including the harbour. We simulate the wave field and the nearshore currents produced by the primary sector incoming waves coming from 260° North, with wave height of 3m and a wave period of 10s. We are interested in the hydrodynamic fields produced by the interaction between the abovementioned incoming wave train and the coastal structures of the Cetraro harbour. The numerical simulations are carried out on a boundary conforming curvilinear grid (Figure 2) which reproduces the coastal region opposite Cetraro harbour.

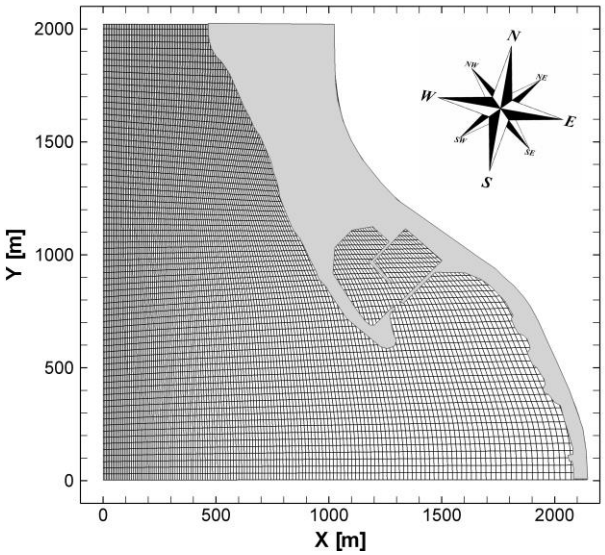

Fig. 2: Curvilinear calculation grid. Coastal region opposite to the Cetraro harbour. Only one coordinate line out of four is shown.

In Figure 3(a) a plane view of an instantaneous wave field is shown. From this figure it is possible to see the refraction (variation in the direction) which the wave fronts coming from the West sector undergo, due to the interaction with the shallow seabeds. It is also possible to observe, in the quadrant delimited by 450m<X<950m and 900m<Y<2000m, the shoaling and breaking effects which the incoming wave trains undergo as they propagate towards the shoreline and, in the quadrant delimited by 450m<X<1100m and 0m<Y<900m, the reflection effects produced by the interaction of the above-mentioned wave trains and the vertical wall of the main jetty. In Figure 3(b) a detailed plane view of the instantaneous wave field at the harbour entrance is shown. From this figure it is possible to see the diffraction (significant rotation) which the wave fronts undergo at the extremity of the main jetty head.

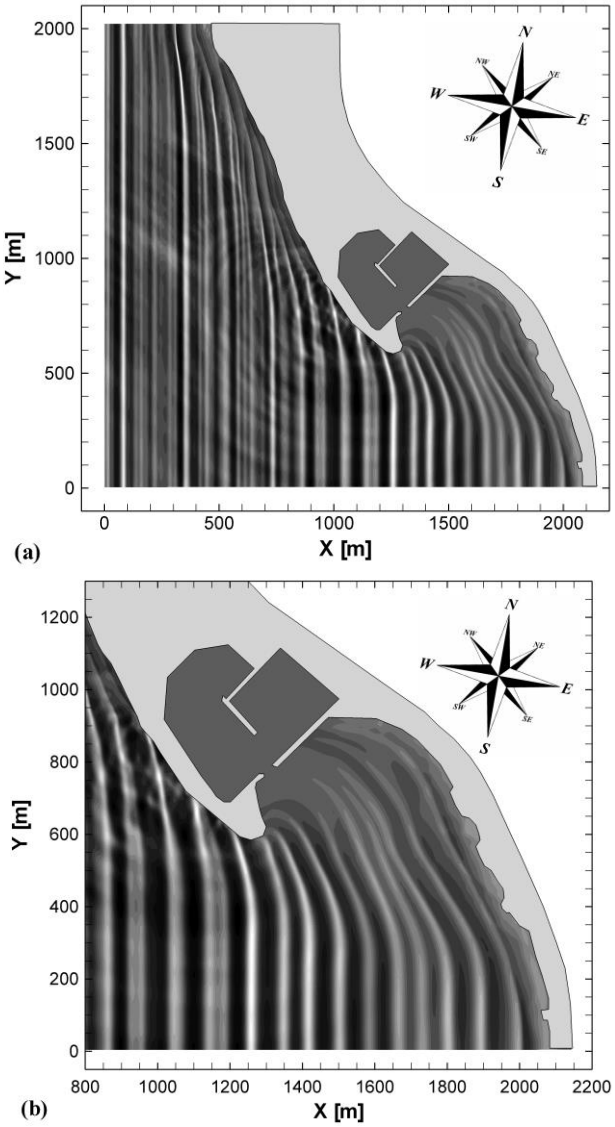

Fig. 3: (a) Instantaneous wave field in the coastal region opposite to the Cetraro harbour. (b) Detail.

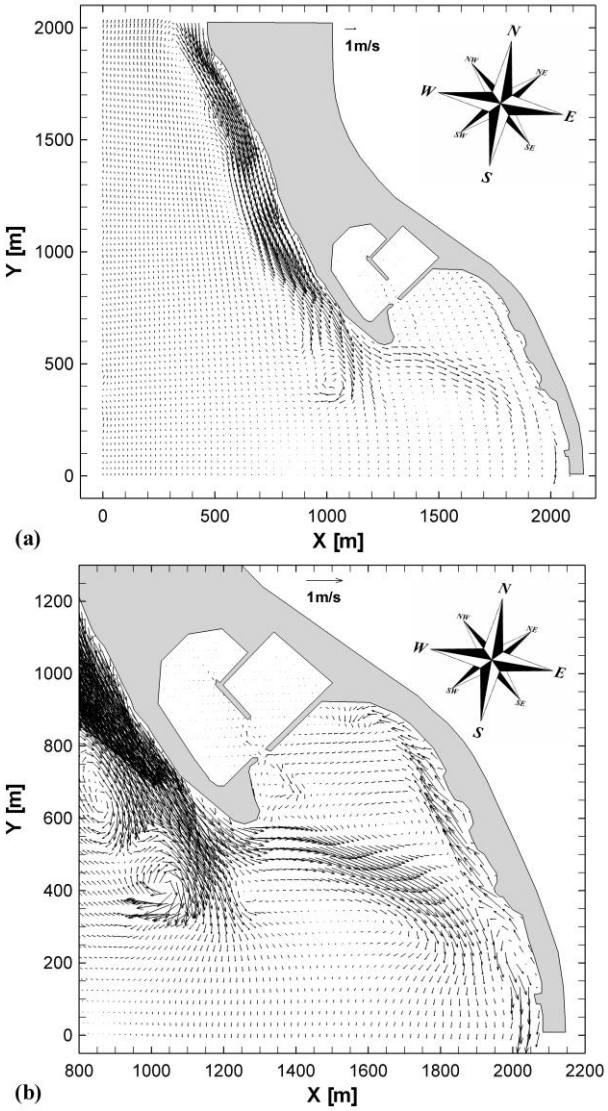

Fig. 4: (a) Time averaged velocity field in the coastal region opposite the Cetraro harbour. A vector out of ten is represented in the x direction and a vector out of four is represented in the y direction. (b) Detail. A vector out of four is represented.

In Figure 4(a) the time-averaged velocity field in the coastal region opposite Cetraro harbour is shown. From this figure it can be noticed that the wave trains obliquely approaching the shoreline give rise to a longshore current which propagates from North-West to South-East. In Figure 4(b) a detail of the time-averaged velocity field at the entrance of the harbour is shown. From this figure, it is possible to see that a large counter-clockwise recirculation eddy forms in the area opposite the harbour entrance. Upstream of the reattachment point of the eddy (point where the main current reconnects with the shoreline), located South-East of the harbour entrance (around X=1900m and Y=500m), a secondary longshore current heading North-West can be observed. Downstream of the above-mentioned reattachment point, the main longshore current heading South-East strongly recovers.

As can be seen in Figs. 4(a) and 4(b), the highest current velocities occur in the coastal region North-West of the harbour. From this area, sediment particles are put into suspension by the breaking waves and are carried away by the heading South-East main current. A part of the sediment load settles along the path of the main current; the other part reaches the reattachment point of the recirculation eddy. From this point, the sediment load is carried partially towards South-East by the main current and partially towards the entrance of the harbour by the secondary longshore current that characterises the recirculation eddy. In this eddy, the sediment load which is carried by the secondary current tends to settle close to the entrance of the harbour, where the wave energy and the current velocity are low. From

this, it can be deduced that the silting which affects the Cetraro harbour area is due to the sediment load coming from the coastal region North-West of the harbour and the presence of the recirculation eddy characterised by a heading North-West longshore current which is able to carry part of the sediment load towards the entrance of the harbour. In summary, in the above coastal region, sediment transport, seabed erosion and coastline changes are substantially affected by the longshore current coming from North-West and by the recirculation eddy. However, it cannot be excluded the secondary contribution to the silting in the entrance harbour area due to nearshore currents induced by wave trains coming from South and South-West.

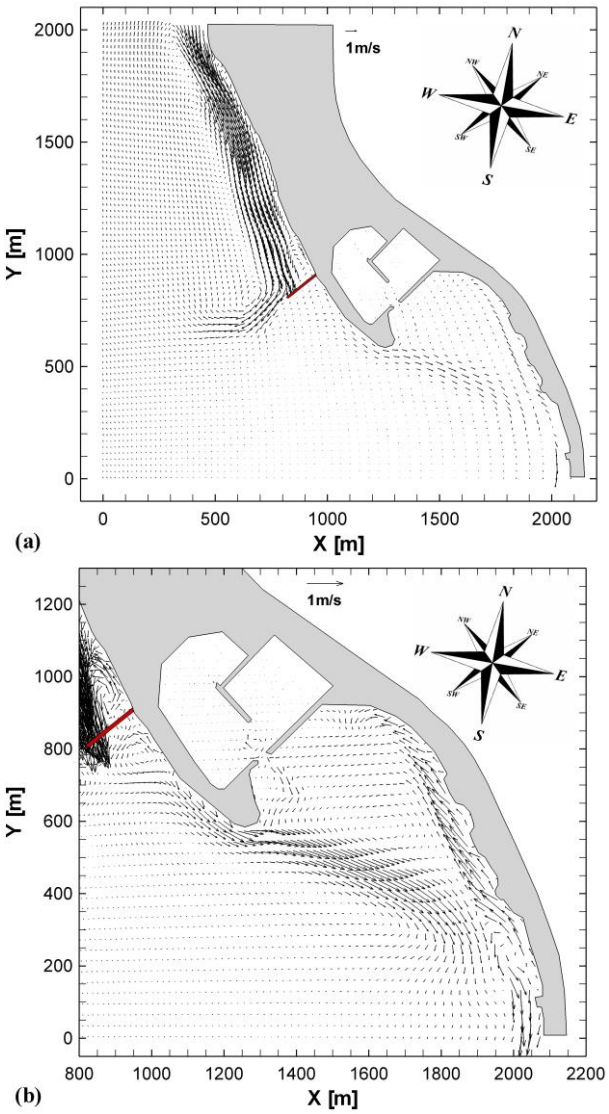

Fig. 5: (a) Time averaged velocity field in the coastal region opposite the Cetraro harbour in presence of the groin (highlighted in red). A vector out of ten is represented in the x direction and a vector out of four is represented in the y direction. (b) Detail. A vector out of four is represented.

Figures 5(a) and 5(b) show respectively a plane view and a detailed view of the time-averaged velocity fields that take place in the case in which, updrift to the head of the main jetty, a 150m long groin is built. From Fig. 5(a) it can be noticed that the groin partially intercepts the longshore current coming from North-West. From Fig. 5(b) it is observed that downdrift of the groin a small counter-clockwise eddy takes place. Moreover, from the same figure it is observed that, also in this case, due to the obliquely incident waves, downdrift of the jetty head, a main longshore current (heading South-East) and a counter-clockwise recirculation eddy take place. As in the previous case, updrift of the recirculation eddy reattachment point, close to the shoreline, a secondary longshore current occurs, while downdrift of the reattachment point the heading South-East main longshore current takes place. From the comparison between Fig. 4(a) and Fig. 5(a) it can be deduced that the blocking effect produced by the groin on the longshore current coming from North-West does not modify the pattern of the nearshore currents in the area downdrift the jetty head and in the one opposite the harbour entrance.

The presence of the groin produces seabed erosion downdrift of the groin and erosion of the coastline South-East of the harbour entrance. In fact, the presence of the groin significantly reduces, with respect to the previous case, the contribution of sediment coming from the coastal area North-West of the harbour. In particular, near to the recirculation reattachment point, the breaking waves is significant and puts into suspension the solid particles, which are partially transported to North-West by the secondary longshore current and partially to South-East by the main longshore current. In this case, the reduction of sediment contribution coming from the coastal area updrift of the groin implies that the balance between the sediment coming from North-West and the sediment put into suspension by the breaking waves and carried away by the longshore currents is negative. From this it follows that, near to the reattachment point of the recirculation eddy and, more in general, in the coastal area South-East of the harbour entrance, seabed and coastline erosion take place.

On the basis of these considerations, it is possible to deduce that the construction of the above groin, despite it could reduce the sedimentation of solid particles coming from North-West in the coastal area opposite the harbour entrance, induces an increase in the seabed erosion downdrift of the groin and coastline erosion in proximity of the reattachment point and in the coastal area South-East of the harbour entrance.

4 Conclusion

A model based on an integral and contravariant form of the fully non-linear Boussinesq equations and the non-linear shallow water equations on generalized curvilinear grids has been presented. The proposed contravariant form of the motion equations is devoid of the Christoffel symbols and is numerically integrated by means of a high-order shock-capturing WENO scheme that uses an exact Riemann solver. This model can be used for the simulation of wave fields and nearshore currents in the coastal region characterized by morphologically complex coastal lines and irregular seabed and by the presence of coastal structures.

The proposed model has been applied to a real case of engineering interest. With this model, wave fields and wave-induced nearshore currents have been simulated in the coastal region opposite Cetraro harbour (Italy). The numerical results give a representation of the hydrodynamic phenomena which contribute to generate the silting process at the entrance of the Cetraro harbour. Finally, wave fields and wave-induced nearshore currents have been simulated in the presence of a 150m long groin placed updrift of the head of the main jetty. Such simulations have been used to evaluate the effects induced by the groin on the sediment transport phenomena.

References:

[1] Aris, R., *Vectors, tensors, and the basic equations of fluid mechanics*, New York, USA, Dover, 1989.

[2] Cannata, G., Lasaponara, F. & Gallerano, F., Non-Linear Shallow Water Equations numerical integration on curvilinear boundary-conforming grids, *WSEAS Transactions on Fluid Mechanics*, No. 10, 2015, pp. 13-25.

[3] Cannata, G., Petrelli, C., Barsi, L., Camilli, F. & Gallerano, F., 3D free surface flow simulations based on the integral form of the equations of motion, *WSEAS Transactions on Fluid Mechanics*, No. 12, 2017, pp. 166-175.

[4] Cannata, G., Petrelli, C., Barsi, L., Fratello, F. & Gallerano, F., A dam-break flood simulation model in curvilinear coordinates, *WSEAS Transactions on Fluid Mechanics*, No. 13, 2018, pp. 60-70.

[5] Chen, Q., Fully nonlinear Boussinesq-type equations for waves and currents over porous bed, *Journal of Engineering Mechanics*, No. 132(2), 2006, pp. 220-230.

[6] Gallerano, F., Cannata, G. & Tamburrino, M., Upwind WENO scheme for shallow water equations in contravariant formulation, *Computers & Fluids*, No. 62, 2012, pp. 1-12.

[7] Gallerano, F., Cannata, G. & Lasaponara, F., Numerical simulation of wave transformation, breaking run-up by a contravariant fully nonlinear Boussinesq model, *Journal of Hydrodynamics B*, No. 28, 2016, pp. 379-388.

[8] Gallerano, F., Cannata, G. & Lasaponara, F., A new numerical model for simulations of wave transformation, breaking and longshore currents in complex coastal regions, *International Journal for Numerical Methods in Fluids*, No. 80, 2016, pp. 571-613.

[9] Gallerano, F., Cannata, G., Lasaponara, F. & Petrelli, C., A new three-dimensional finite-volume non-hydrostatic shock-capturing model for free surface flow, *Journal of Hydrodynamics*, No. 29(4), 2017, pp. 552-566.

[10] Gallerano, F., Pasero, E. & Cannata, G., A dynamic two-equation sub grid scale model, *Continuum Mechanics and Thermodynamics*, No. 17(2), 2005, pp. 101-123.

[11] Keshtpoor, M., Puleo, J. A., Shi, F. & Ma, G., 3D numerical simulation of turbulence and sediment transport within a tidal inlet, *Coastal Engineering*, No. 96, 2015, pp. 13-26.

[12] Luo, H. & Bewley, T. R., On the contravariant form of the Navier–Stokes equations in time-dependent curvilinear coordinate systems, *Journal of Computational Physics*, No. 199(1), 2004, pp. 355-375.

[13] Ma, G., Shi, F. & Kirby, J.T., Shock-capturing non-hydrostatic model for fully dispersive surface wave processes, *Ocean Modelling*, No. 43-44, 2012, pp. 22-35.

[14] Nwogu, O., An alternative form of the Boussinesq equations for near shore wave propagation, *Journal of Waterway, Port, Coastal and Ocean Engineering*, No. 119(6), 1993, pp. 618-638.

[15] Roeber, V. & Cheung, K. F., Boussinesq-type model for energetic breaking waves in fringing reef environments, *Coastal Engineering*, No. 70, 2012, pp. 1-20.

[16] Rossmanith, J.A., Bale, D.S. & LeVeque, R.J., A wave propagation algorithm for hyperbolic systems on curved manifolds, *Journal of Computational Physics*, No. 199(2), 2004, pp. 631-662.

[17] Shi, F., Kirby, J. T., Harris, J. C., Geiman, J. D., & Grilli, S. T., A high-order adaptive time-stepping TVD solver for Boussinesq modeling of breaking waves and coastal inundation, *Ocean Modelling*, No. 43, 2012, pp. 36-51.

[18] Shi, F., Kong, Y. & Ding, P., An implicit method using contravariant velocity components and calculations in a harbour-channel area, *ACTA Oceanologica Sinica*, No. 17(4), 1998, pp. 423-432.

[19] Tonelli, M. & Petti, M., Hybrid finite-volume finite-difference scheme for 2HD improved Boussinesq equations, *Coastal Engineering*, No. 56, 2009, pp. 609-620.

[20] Tonelli, M., & Petti, M., Shock-capturing Boussinesq model for irregular wave propagation, *Coastal Engineering*, No. 61, 2012, pp. 8-19.

[21] Toro, E., *Shock-capturing methods for free-surface shallow flows*, John Wiley and Sons: Manchester, 2001.

[22] Wei, G., Kirby, J. T., Grilli, S. T., & Subramanya, R., A fully nonlinear Boussinesq model for surface waves. Part 1. Highly nonlinear unsteady waves, *Journal of Fluid Mechanics*, No. 294, 1995, pp. 71-92